Evolution of Stimulated Raman into Stimulated Compton Scattering of Laser Light via Wave Breaking of Plasma Waves

M. J. Everett, A. Lal, D. Gordon, K. Wharton, C. E. Clayton, W. B. Mori, and C. Joshi
Electrical Engineering Department, University of California, Los Angeles, California 90024
(Received 3 August 1994)

Experimental evidence for the evolution of stimulated Raman backscatter instability of laser light into stimulated Compton scattering in an initially cold plasma is presented using time and wave number resolved spectra, $w(t)$ and $w(k)$, of Thomson scattered light from plasma fluctuations. Supporting particle simulations show that the key to the spectral evolution is wave breaking of Raman plasmons, which accelerates some electrons up to 4 times the phase velocity, and the consequent return current of the bulk plasma electrons in the opposite direction.

PACS numbers: 52.35.Mw, 52.40.Nk, 52.50.Jm

When an intense laser pulse interacts with an underdense plasma, a number of parametric instabilities can be excited [1]. These instabilities have been under intense investigation for over a decade because of their role in laser fusion [2] and laser-driven collective plasma accelerators [3]. Experimentally, there is now ample evidence for these instabilities, yet their nonlinear evolution via wave-particle and wave-wave interactions remains poorly documented in experiments. In this Letter we show, using experimental data and supporting simulations, how one such instability, stimulated Raman backscattering (SRS) [4], evolves into stimulated Compton scattering (SCS) [5] via wave breaking of Raman plasmons.

The SRS and SCS instabilities can be viewed as the low- and high-plasma-temperature regimes of the same instability, consisting of an incident laser (w_0, k_0), a backscattered light beam (w_b, k_b), and an electron plasma wave (w, k), where $w = w_0 - w_b$, $k = k_0 + k_b$. The dispersion relation which describes both instabilities is well known and given by [6]

$$1 + \chi_e = -\frac{\chi_e}{4} k^2 v_0^2 (w_b^2 - w_p^2 - c^2 k_b^2)^{-1} \qquad (1)$$

with

$$\chi_e = \frac{-w_p^2}{k^2} \int \frac{\partial \hat{f}_0 / \partial v}{v - w/k} \, \partial v \,, \qquad (2)$$

where the anti-Stokes term has been dropped. For a Maxwellian plasma the velocity distribution function $\hat{f}_0$ is given by $\hat{f}_0 = \exp(-v^2/2v_{\rm th}^2)/v_{\rm th}\sqrt{2\pi}$, where $v_{\rm th} = \sqrt{kT/m}$ is the electron thermal velocity.

SRS occurs when $k\lambda_D < 1/\sqrt{3}$ where $\lambda_D = v_{\rm th}/w_p$ is the plasma Debye length. It is a coherent response of the entire plasma characterized by a relatively narrow frequency spectrum at $w^2 = w_p^2 + 3k^2 v_{\rm th}^2$ with a dispersion relation $\partial w/\partial k = -c/2$ where c is the speed of light [6]. The SCS instability ($k\lambda_D > 1/\sqrt{3}$) is primarily an interaction between "resonant" electrons (those electrons traveling near the phase velocity w/k of the plasma wave) and the light waves. It is characterized by a broad spectrum and a dispersion relation $\partial w/\partial k = -c$.

Previously, the saturation of SRS via wave breaking has been seen in computer simulations [7], and both SRS [8] and SCS [9] have been seen in experiments. In this Letter, we document the self-consistent evolution of SRS into SCS by actually measuring the w and k spectrum of the plasma waves. We find that the spectrum is initially reasonably consistent with what is expected from strongly driven SRS, but evolves into a broad SCS spectrum. We also observe this in computer simulations which show that the broadening of the spectrum coincides with the wave breaking of the plasma wave.

We begin with the experiment. A CO_2 laser first creates the plasma by tunnel ionization of static gas, 71 mTorr H_2, and then drives the instabilities in the plasma. The laser produces about 60 J of 10.6 μm light per pulse with a rise time of about 150 ps and a FWHM of about 300 ps. The linearly polarized laser is focused using an $f/11.5$ off-axis parabolic mirror to a spot diameter $(1/e)$ of 300 μm which is about $4c/w_p$ wide. The peak focal spot intensity thus approaches 6×10^{14} W/cm^2 or in normalized units $v_0/c = eE/mw_0c \approx 0.2$. Here E is the electric field of the laser. The gas is fully ionized within the first 20 ps by the laser over approximately ± 1 cm on either side of the best focus, producing a plasma density of 4.7×10^{15} cm^{-3} or n/n_c of 4.7×10^{-4}. Based on tunnel ionization theory [10], the initial plasma temperature at ionization is about 75 eV in the direction of polarization of the laser and less than 1 eV in the other two directions [11]. The actual longitudinal temperature based on the experimental results is 6–10 eV, indicating some transfer of energy from the transverse direction. Ion effects play a minimal role because the laser pulse is only five ion periods (ν_{pi}^{-1}) long.

We use collective Thomson scattering to measure the plasma density fluctuations associated with SRS and SCS [8]. The incident angle of the 2 ns (FWHM), 50 MW, 0.53 μm optical probe beam is chosen such that the incident $(w_{\rm pr}, k_{\rm pr})$ and the scattered light (w_s, k_s) will k match to the Raman and Compton waves. To gain the

maximum information about the SRS and SCS density fluctuations in the plasma, we resolve the frequency of scattered light in both time $w(t)$ and wave number $w(k)$. By resolving the evolution of the frequency spectrum versus time $w(t)$, we observe signatures of the growth and breaking of Raman plasmons and their evolution into Compton. The $w(k)$ resolved measurements, on the other hand, allow us to associate a wave number with each frequency in the time resolved data and show for the first time the dispersion relation for the SCS fluctuations.

Thomson scattering of a probe laser from the plasma measures both w and k of the density perturbations as a function of time because the scattered light is shifted by the w and k of the plasma wave. However, as the data must be collected on a camera which has only two dimensions, the frequency spectrum can be measured only as a function of time or wave number, not both in a single laser shot.

For $w(t)$ resolved measurements of the plasma waves, it is necessary to collect a range of scattering angles and reimage them to a small spot which can then be dispersed in w and t. This is accomplished by using a probe beam which is spherically focused by an $f/30$ lens to a 200 μm diameter in the center of the plasma. A lens at the correct k scattering angle then collects the k spectrum of interest and images it onto the input slit of an imaging spectrometer. The output spectrum from the spectrometer is dispersed in time on the other axis by a streak camera with a 20 ps resolution producing the $w(t)$ spectrum shown in Fig. 1(a). This setup cannot be used for fine k resolved measurements because its k resolution is limited by the cone angle of the probe beam to $2\pi/\lambda_{pr} f^{\#} = 0.4\ \mu\text{m}^{-1}$, while the required k resolution is better than $w_p/c = 1.5 \times 10^{-2}\ \mu\text{m}^{-1}$.

To obtain $w(k)$ resolved spectra with adequate k resolution for a single shot determination of the dispersion relation, we use a cylindrically focused probe laser. The

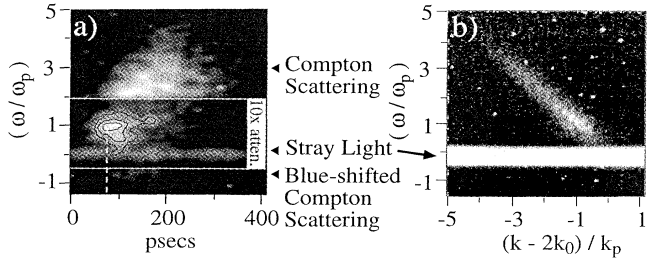

FIG. 1. Log plots of single shot SRS and SCS spectra measured by a Thomson scattered probe beam. (a) Time resolved spectrum showing evolution of SRS into SCS through wave breaking. Central region bounded by the two solid white lines is 10 times attenuated. Contour lines are at $\frac{3}{4}$, $\frac{3}{8}$, and $\frac{3}{16}$ of peak scattering intensity. Dotted line indicates time at which Raman amplitude was measured. (b) Wave number and frequency resolved signal showing the broad Compton scattering spectrum with the characteristic SCS dispersion relation $\partial w/\partial k = -c$. Here $k_p = w_p/c$.

6 mm long line focus minimizes the perpendicular k spread of the laser on one axis, allowing high k resolution in that direction [Fig. 1(b)]. For this case, the quality of the probe beam and optics limit the k resolution to about $5 \times 10^{-3}\ \mu\text{m}^{-1}$, 80 times better resolution than the conventional experimental setup using a spherical lens and 3 times finer than w_p/c. These are the most detailed $w(k)$ spectra obtained in any laser-plasma experiment to date.

The basic features of the time and wave number resolved spectra shown in Figs. 1(a) and 1(b) are as follows. The spectrum is time resolved with a frequency resolution of $0.2w_p$ in Fig. 1(a). It begins with a relatively intense burst of Raman shown by the inner contour line that peaks at approximately the w_p corresponding to fully ionized density. This implies that the plasma is relatively cold and the thermal correction to the Bohm-Gross frequency is small. The deconvolved bandwidth of the Raman, measured as $\approx 0.25w_p$ (FWHM), is dominated by strong coupling of the intense laser. Its width corresponds to eight e-foldings of the spectral growth curve given by the numerical solution to Eq. (1) with a laser v_0/c fixed at 0.1, the average normalized amplitude of the laser over the growth of SRS which occurs immediately following the ionization. A scan taken through these data at time $t = 70$ ps gives a maximum density fluctuation level $\hat{n}/n_0 = 8\%-15\%$ using the usual Bragg scattering formula [12]. Assuming that this level is determined by wave breaking [13] (to be justified later), we can infer a $k\lambda_D$ for the Raman wave of 0.31 to 0.4 and thus a plasma temperature of between 6 and 10 eV.

The intense portion of this burst splits into two components, one shown by the second contour that rapidly decreases in frequency and the other, seen most clearly in the third contour, that remains near w_p. We will show by comparison to particle-in-cell (PIC) simulations later that the component which shows a sudden decrease in frequency is characteristic of wave breaking of the two-dimensional Raman oscillation on axis (where it presumably has the largest amplitude). Coincident with this, the Thomson scattering shows the development of a weaker but much broader spectrum which eventually extends to $0.7w_p$ on the blue side and $4.5w_p$ on the red side of zero frequency. We believe this spectrum is a result of Compton scattering in the non-Maxwellian plasma.

The wave number resolved frequency spectrum, shown in Fig. 1(b), is dominated by the Compton scattering because it is a time integrated spectrum and Compton lasts much longer than the initial Raman burst. The most striking feature of this spectrum is that the slope is $\partial w/\partial k = -c$, showing that it is indeed Compton.

In order to understand the details of the evolution of the Raman fluctuations into Compton fluctuations, we have used the PIC code WAVE [14] because the plasma is neither Maxwellian nor linear during the evolution of SRS into SCS. In order to model the key features of the experiment, we use $k\lambda_D$ as the key parameter in PIC

simulations with a reduced frequency ratio $w_0/w_p = 5$ because of computational limitations. In the simulations we use $k\lambda_D = 0.38$ (corresponding to the plasma temperature in the experiment of 9 eV), $v_0/c \approx 0.2$ peak, and a pulse which rises in $300w_p^{-1}$ and then remains constant. The simulation box is $100c/w_p$ long along the direction of propagation of the laser. Taking a Gabor transform [15] of the density at one point in the plasma provides the amplitude of each frequency component of the SRS and SCS density perturbations as a function of time [Fig. 2(a)], just as the spectrometer and streak camera combination does in the experiment. The discontinuity at zero frequency is a subtlety of the Gabor transform which has no effect on the overall spectrum. Also, to better visualize the evolution of SRS into SCS it is instructive to look at the temporal evolution of the $w(k)$ spectrum of plasma waves. This is done by breaking the time history of the plasma waves into sections that are each $80w_p^{-1}$ long and then Fourier transforming them in time and space to produce the snapshots of the $w(k)$ spectrum of the plasma waves. Three snapshots taken at $200w_p^{-1}$ when the predominant mode is SRS, at $280w_p^{-1}$ when SRS is wave breaking and evolving into SCS, and at $360w_p^{-1}$ when SCS is fully developed are shown in Figs. 2(b), 2(c), and 2(d). The interpretation of the $w(t)$ and $w(k)$ plots of Fig. 2 is aided by the phase space (v_x/v_{ph} vs space) and (v_x/v_{ph} vs time) plots, where v_{ph} is the theoretical phase velocity of the plasmons before wave breaking and x is the direction of propagation of the laser beam. One such example is shown in Figs. 3(a) and 3(b) taken at $280w_p^{-1}$ when wave breaking occurs.

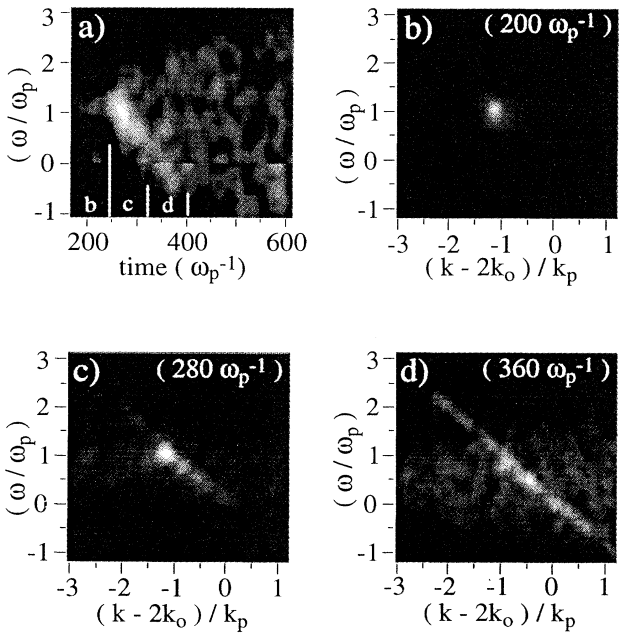

FIG. 2. Simulation results showing evolution of SRS into SCS through wave breaking. (a) Time resolved frequency spectrum of plasma density fluctuations near $2k_0$ associated with SRS and SCS. Snapshots taken over intervals marked in plot (a) showing $w(k)$ spectrum of (b) Raman instability, (c) wave breaking, and (d) Compton spectrum with blueshifted components. Spectra (b), (c), and (d) are all on the same scale, also showing the increase of background noise around $2k_0$ caused by wave breaking.

As in the experiment [Fig. 1(a)], one sees SRS growing rapidly at $w = w_p$ and $k = 2k_0 - w_p/c$ in the simulations [Figs. 2(a) and 2(b)]. Its bandwidth is narrower than in the experiments because the driving term from Eq. (1), v_0k, is 5 times lower and the range of unstable modes is equal to twice the peak growth rate. The SRS begins to trap electrons once it grows to an amplitude of about 10%, in good agreement with the warm plasma wave-breaking theory [13]. These density perturbations continue to grow somewhat until the waves break. The onset of wave breaking occurs at $280w_p^{-1}$. It is characterized by, first, roughly 20% of the electrons being accelerated in the forward direction by the plasma wave and, second by the bulk of the plasma moving backwards, generating a return current. This is clearly visible in Figs. 3(a) and 3(b). At wave breaking, some electrons are seen to gain velocities up to $3v_{ph}$, while the bulk of the plasma at this time is moving backwards at $v_b = 0.3v_{ph}$. Note that at this time there is still an oscillation at w_p [Fig. 2(c)]; however, its k spectrum is rapidly evolving from a well-defined Bohm-Gross peak at $2k_0 - w_p/c$ into a much broader spectrum. The accelerated electrons are still very much bunched at the Raman wave number [Fig. 3(b)]. Consequently, SCS does not have to grow from noise. The electron distribution function [Fig. 3(a)] at this time is far from Maxwellian. In fact, it more closely resembles a bi-Maxwellian with a colder Maxwellian containing 80% of the particles drifting backwards in the laboratory frame and a second hotter Maxwellian containing 20% of the electrons drifting forward. Eventu-

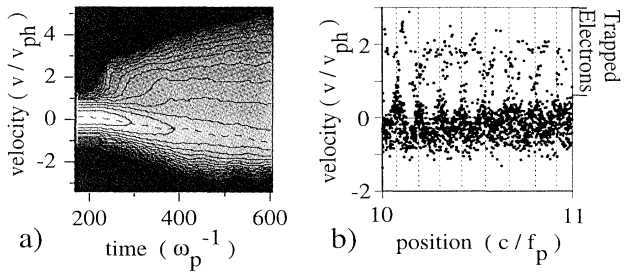

FIG. 3. Velocity phase space plots for simulation. Velocity axis is normalized to $v_{ph} = w_p/(2k_0 - k_p)$, the initial phase velocity of the Raman wave. (a) Evolution of velocity distribution function (log plot, 5 contours per factor of 10) from a relatively cold Maxwellian to a much hotter non-Maxwellian consisting of trapped electrons moving forward with phase velocities up to $4v_{ph}$ and the main body of the electrons moving backward. The dotted line tracks the peak of the distribution function. (b) Scatter plot of electron velocity versus position showing periodicity of electron trapping at the wave number of the Raman, taken at $280w_p^{-1}$.

ally some electrons are accelerated up to 4 times the phase velocity of the SRS plasmons. The return current that results from wave breaking alters the $w(t)$ evolution. As shown in Fig. 2(a), the bright SRS peak rapidly decreases in frequency, similar to one of the observed features in the experiment. This occurs because the primary response of the plasma is given by the cold electrons. As these electrons are moving toward the laser, in the opposite direction of the plasma wave, the plasma frequency is Doppler shifted in the laboratory frame by a factor $1 - v_b/v_{\rm ph}$. In addition, the effective plasma density is reduced as the response of the hot electrons at the cold Raman frequency is small. This second effect is less important than the Doppler shift. Immediately after wave breaking, the plasma spectrum rapidly broadens, a characteristic of SCS. The relationship between w and k for this spectrum shown in Figs. 2(c) and 2(d) confirms that the wave has indeed evolved into Compton after being heated by the Raman wave breaking.

An important difference between the simulations and the experiment is that the simulations are one dimensional (1D) whereas the experiment is 3D. Since the laser beam in the experiment has a transverse intensity profile that falls off as one moves away from the center, we expect the SRS wave to grow and break close to the center. This wave breaking causes the return current to flow in the center region roughly c/w_p wide. It is in this region where the SRS frequency drops for the reasons described above. Away from the beam center, the plasma wave takes longer to break, thus producing the continuing enhancement of the spectrum near w_p in the experiment. The neglect of ion motion in the transverse direction in these 1D simulations (which precludes filamentation for instance) is not believed to be a serious concern since the laser rise time is only about two ion periods long [16].

The crucial experimental confirmation that SRS evolution into SCS occurs via wave breaking, which accelerates electrons and thus drives a return current, is the appearance of blueshifted components of the Compton scattering seen both in the experiment and in the simulations [Fig. 1(a) and Fig. 2(a)]. These correspond to density fluctuations that are actually moving back toward the laser in the laboratory frame. The theoretical growth rate is zero for these fluctuations for a Maxwellian plasma. However, numerical solutions to Eq. (1) for non-Maxwellian plasmas show that growth of the blueshifted Compton scattering occurs when a region on the negative velocity side of the electron distribution function has a negative slope ($\partial \hat{f}_0/\partial v < 0$ with $v < 0$). Such is the case when the return current in effect produces a backward-drifting distribution function.

The evolution of SCS, $w(t)$, and $w(k)$, is qualitatively similar in both the experiment and simulations. At $360 w_p^{-1}$, the $w(k)$ snapshot [Fig. 2(d)] shows the dispersion relationship of the SCS waves with a negative speed of light slope, as does the experiment [Fig. 1(b)]. The simulations which are a snapshot in time again show the blueshifted frequency components which are not discernible in the time integrated $w(k)$ plot of Fig. 1(b). In a thermal plasma the SCS always has a maximum growth rate at $w > w_p$. However, both the $w(t)$ and $w(k)$ space [Figs. 1(a) and 1(b)] show Compton peaking close to $0.7 w_p$. If the main body of the electrons constituting the return current were to move backwards at $v_{\rm ph}$, then the peak of the SRS and SCS fluctuations would be close to zero frequency. The peak in the experiment near $0.7 w_p$ indicates that the main body of the electrons is traveling backwards at less than the initial Raman phase velocity, a conclusion supported by the phase space plots of Fig. 3 and $w(k)$ plots of Fig. 2(d).

In conclusion, we have documented the evolution of the stimulated Compton scattering instability in an initially cold plasma. Stimulated Raman scattering occurs first. The SRS plasmons trap background plasma electrons which are both bunched at the correct k for SCS and accelerated over a broad velocity range up to $4 v_{\rm ph}$. At the same time the bulk of the plasma electrons drift backward to maintain charge neutrality. The SCS spectrum is then determined by this resulting nonthermal electron distribution.

This work was supported by Department of Energy Grant DE-AS03-83-ER40120.

[1] J. F. Drake *et al.*, Phys. Fluids **17**, 778 (1974).
[2] W. L. Kruer, *The Physics of Laser Plasma Interactions* (Addison-Wesley Publishing Co., Redwood City, CA, 1988).
[3] C. Joshi *et al.*, Nature **311**, 525 (1984).
[4] A. Offenberger *et al.*, Phys. Rev. Lett. **49**, 371 (1982); H. A. Baldis *et al.*, Phys. Rev. Lett. **62**, 2829 (1989); R. P. Drake and S. H. Batha, Phys. Fluids B **3**, 2936 (1991).
[5] A. T. Lin and J. M. Dawson, Phys. Fluids **18**, 201 (1975); R. P. Drake *et al.*, Phys. Rev. Lett. **64**, 423 (1990).
[6] D. W. Forslund *et al.*, Phys. Fluids **18**, 1002 (1975); K. Estabrook and W. L. Kruer, Phys. Fluids **26**, 1892 (1983).
[7] H. H. Klein *et al.*, Phys. Fluids **18**, 1031 (1975); D. W. Forslund *et al.*, Phys. Fluids **18**, 1002 (1975).
[8] D. M. Villeneuve *et al.*, J. Opt. Soc. Am. B **8**, 895 (1991).
[9] W. P. Leemans *et al.*, Phys. Rev. Lett. **67**, 1434 (1991).
[10] L. V. Keldysh, Sov. Phys. JETP **20**, 1307 (1965).
[11] W. P. Leemans *et al.*, Phys. Rev. Lett. **68**, 321 (1992).
[12] R. E. Slusher and C. M. Surko, Phys. Fluids **23**, 1974 (1980).
[13] T. P. Coffey, Phys. Fluids **14**, 1402 (1971).
[14] R. L. Morse and C. W. Nielson, Phys. Fluids **14**, 830 (1971).
[15] S. Qian and D. Chen, IEEE Trans. Signal Proc. **41**, 2429 (1993).
[16] M. Dunne *et al.*, Phys. Rev. Lett. **72**, 1024 (1994).

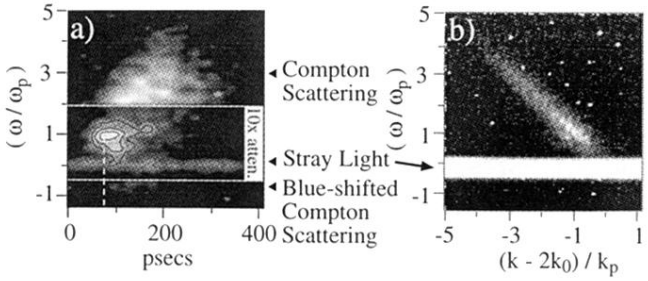

FIG. 1. Log plots of single shot SRS and SCS spectra measured by a Thomson scattered probe beam. (a) Time resolved spectrum showing evolution of SRS into SCS through wave breaking. Central region bounded by the two solid white lines is 10 times attenuated. Contour lines are at $\frac{3}{4}$, $\frac{3}{8}$, and $\frac{3}{16}$ of peak scattering intensity. Dotted line indicates time at which Raman amplitude was measured. (b) Wave number and frequency resolved signal showing the broad Compton scattering spectrum with the characteristic SCS dispersion relation $\partial w/\partial k = -c$. Here $k_p = w_p/c$.

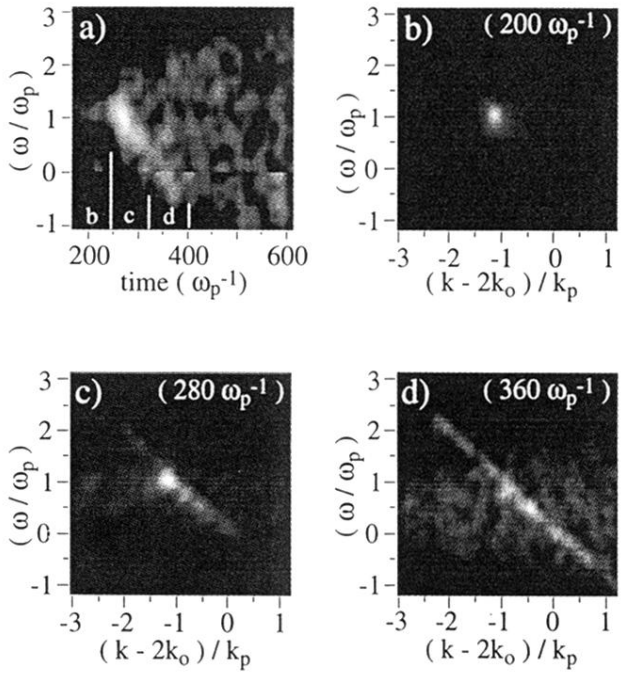

FIG. 2. Simulation results showing evolution of SRS into SCS through wave breaking. (a) Time resolved frequency spectrum of plasma density fluctuations near $2k_0$ associated with SRS and SCS. Snapshots taken over intervals marked in plot (a) showing $w(k)$ spectrum of (b) Raman instability, (c) wave breaking, and (d) Compton spectrum with blueshifted components. Spectra (b), (c), and (d) are all on the same scale, also showing the increase of background noise around $2k_0$ caused by wave breaking.

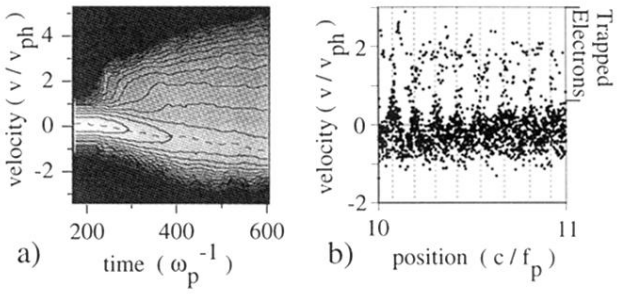

FIG. 3. Velocity phase space plots for simulation. Velocity axis is normalized to $v_{\rm ph} = w_p/(2k_0 - k_p)$, the initial phase velocity of the Raman wave. (a) Evolution of velocity distribution function (log plot, 5 contours per factor of 10) from a relatively cold Maxwellian to a much hotter non-Maxwellian consisting of trapped electrons moving forward with phase velocities up to $4v_{\rm ph}$ and the main body of the electrons moving backward. The dotted line tracks the peak of the distribution function. (b) Scatter plot of electron velocity versus position showing periodicity of electron trapping at the wave number of the Raman, taken at $280w_p^{-1}$.